Structural transformations of Li2C2 at high pressures

Structural transformations of Li_2C_2 at high pressures

Ilias Efthimiopoulos,[1] Daryn E. Benson,[2] Sumit Konar,[3] Johanna Nylén,[3] Gunnar Svensson,[3] Ulrich Häussermann,[3,*] Stefan Liebig,[4] Uwe Ruschewitz,[4] Grigory V. Vazhenin,[1] Ingo Loa,[5] Michael Hanfland,[6] and Karl Syassen[1]

[1]*Max-PIanck-Institute for Solid State Research, Heisenbergstrasse 1, D-70569 Stuttgart, Germany*

[2]*Department of Physics, Arizona State University, Tempe, Arizona 85287-1504, USA*

[3]*Department of Materials and Environmental Chemistry, Stockholm University, SE-10691 Stockholm, Sweden*

[4]*Department of Chemistry, University of Cologne, Greinstrasse 6, 50939 Cologne, Germany*

[5]*The University of Edinburgh, School of Physics and Astronomy, Centre for Science at Extreme Conditions (CSEC), King's Buildings, Edinburgh EH9 3FD, United Kingdom*

[6]*European Synchrotron Radiation Facility, 6 Rue Jules Horowitz, F 38000 Grenoble, France*

(Received 6 June 2015; published 19 August 2015)

Structural changes of Li_2C_2 under pressure were studied by synchrotron x-ray diffraction in a diamond anvil cell under hydrostatic conditions and by using evolutionary search methodology for crystal structure prediction. We show that the high-pressure polymorph of Li_2C_2, which forms from the *Immm* ground-state structure ($Z = 2$) at around 15 GPa, adopts an orthorhombic *Pnma* structure with $Z = 4$. Acetylide C_2 dumbbells characteristic of *Immm* Li_2C_2 are retained in *Pnma* Li_2C_2. The structure of *Pnma* Li_2C_2 relates closely to the anticotunnite-type structure. C_2 dumbbell units are coordinated by nine Li atoms, as compared to eight in the antifluorite structure of *Immm* Li_2C_2. First-principles calculations predict a transition of *Pnma* Li_2C_2 at 32 GPa to a topologically identical phase with a higher *Cmcm* symmetry. The coordination of C_2 dumbbell units by Li atoms is increased to 11. The structure of *Cmcm* Li_2C_2 relates closely to the Ni_2 In-type structure. It is calculated that *Cmcm* Li_2C_2 becomes metallic at pressures above 40 GPa. In experiments, however, *Pnma* Li_2C_2 is susceptible to irreversible amorphization.

DOI: 10.1103/PhysRevB.92.064111 PACS number(s): 62.50.−p, 07.35.+k, 63.20.dk, 64.70.km

I. INTRODUCTION

Carbides of alkali and alkaline-earth metals typically occur as saltlike acetylides which consist of C_2^{2-} dumbbell anions isoelectronic to dinitrogen [1]. Recent theoretical studies suggested that acetylide carbides should transform to modifications with polymeric carbon structures at moderate pressures (below 10 GPa) [2–6]. The predicted "polycarbides" consist of carbon polyanions with chain, ribbon, or layer structures which are stabilized by electrostatic interactions with surrounding cations. Such polyanions occur typically in Zintl phases and are well known for, e.g., silicon and germanium. For carbon they represent a hitherto unknown chemical and structural feature. Polycarbides display distinct electronic structures and are predicted to be superconductors [3–5].

Yet the computational predictions deviate notably from results of experimental high-pressure studies. Hitherto investigated Li_2C_2, CaC_2, and BaC_2 have in common that acetylide C_2 dumbbells are retained until irreversible amorphization occurs at pressures far higher than the calculated transition pressures for polymeric carbide formation [7–9]. The discrepancy has been attributed to kinetic hindrance [3]. Prior to amorphization BaC_2 and Li_2C_2 undergo structural transformations at around 4 and 15 GPa, respectively, in room temperature experiments [7–9]. These transformations correspond to a "conventional" increase of coordination numbers with pressure, leading to denser packings of cations and dumbbells. In the ambient-pressure structure of BaC_2 Ba^{2+} and C_2^{2-} ions are six-coordinated and arranged as in the NaCl structure. The rhombohedral high-pressure modification relates to the CsCl structure, with both types of ions attaining an eightfold coordination [7]. For Li_2C_2 the structure of the high-pressure form has not been conclusively characterized [8,9].

Here we present the elucidation of the high-pressure behavior of Li_2C_2 from combined synchrotron diffraction experiments and crystal structure prediction methodology. To prevent the generation of enthalpically more favorable polymeric carbides in the computations, a constrained evolutionary algorithm was employed that enforced retention of C_2 dumbbell units at high pressures [10]. We further show that if amorphization of Li_2C_2 were suppressed, a high-pressure form predicted here would approach metallic behavior at pressures above 40 GPa.

II. METHODS

A. Experiments

All steps of sample preparation were performed in an Ar-filled glove box (H_2O and O_2 concentration <1 ppm). Starting materials for Li_2C_2 synthesis were lithium (ABCR, 99.99%) and graphite powder (Sigma-Aldrich, 99.9998%), which was degassed at 800 °C under dynamic vacuum for 24 h prior to use. Stoichiometric amounts of lithium and graphite were transferred into a purified Ta ampoule. Afterwards the ampoule was sealed in He atmosphere (800 mbar) and was placed inside a quartz ampoule, which was sealed under vacuum. The quartz ampoule was heated for 24 h at 1073 K in air (tube furnace), after which the sample was allowed to cool by turning off the furnace. An air- and moisture-sensitive fine powder with a light-gray color was obtained. The phase purity of the sample was checked by powder x-ray diffraction (PXRD, Huber G670, Cu $K\alpha_1$ radiation, capillary). Apart from a small amount of unreacted graphite, no impurities were detected.

*Corresponding author: ulrich.haussermann@mmk.su.se

In-situ high-pressure monochromatic PXRD experiments were performed with a membrane-driven diamond anvil cell (DAC) using a culet size of 400 microns. Powdered samples were loaded under inert gas atmosphere into a 150-μm-sized hole drilled in a stainless steel gasket. The pressure-transmitting medium (PTM) was helium. Diffraction data were collected at room temperature at the ID09 beamline of the ESRF using a MAR555 flat panel detector. The x-ray wavelength was $\lambda = 0.415\,58$ Å, and the beam diameter on the sample was set to 30 μm. In order to improve powder averaging, the DAC was rocked by ± 3 deg. The pressure was monitored by the ruby luminescence method [11]. The two-dimensional diffraction data were integrated using the software FIT2D [12].

All diffractograms were inspected using the STOE WINXPOW software system [13]. DICVOL [14] within WINXPOW was used for indexing and ENDEAVOUR [15] for an *ab-initio* structural solution using a direct-space approach. Rietveld refinements were performed with GSAS [16]. More details of the structure solution and refinement are given in Sec. III.

B. Computations

Structure searches were carried out using the evolutionary algorithm USPEX [17–19]. The search over configurational space was constrained to structures containing C_2 acetylide units. C-C bond connectivity was enforced using the Z-matrix representation [20] available in the *ab-initio* code SIESTA [21]. However, computationally demanding SIESTA was only used in the initial phase of a search as a means to quickly optimize the structure by constraining the molecular geometry and degrees of freedom of the C_2 acetylide units. These calculations employed the Perdew-Burke-Ernzerhof (PBE) exchange correlation [22] as well as the single-ζ basis set. The plane-wave cutoff was set at 100 Ry, and a Monkhorst-Pack grid defined at a cutoff of 10 Å was used. The pseudopotentials used were Troullier and Martins norm-conserving pseudopotentials [23]. The final stages of a search were performed using the Vienna *Ab Initio* Simulation Package (VASP) [24]. The target pressure for searches was chosen to be 20 GPa. All populations contained 30 structures, and the initial population's structures were randomly generated. All structures contained 16 atoms constrained to the chemical composition of Li_2C_2 (i.e., $Z = 4$).

Enthalpy versus pressure relations of Li_2C_2 phases were calculated using the first-principles all-electron projector augmented waves (PAW) method [25] as implemented in VASP. Exchange-correlation effects were treated within the generalized gradient approximation (GGA) using the PBE parametrization [22]. The structures were relaxed with respect to pressure, lattice parameters, and atomic positions. Forces were converged to better than 1×10^{-3} eV/Å. The integration over the Brillouin zone (BZ) was done on a grid of special k points of size $6 \times 6 \times 6$, determined according to the Monkhorst-Pack scheme and using Gaussian smearing to determine the partial occupancies for each wave function [26]. The kinetic energy cutoff was set to 675 eV. To obtain the band structure and enthalpies, the tetrahedron method with Blöchl correction was employed for BZ integration [27]. Structure relaxations and phonon calculations were performed at pressures ranging from 0 to 40 GPa. Once a structure was relaxed at a target pressure, zone-centered phonon calculations were executed using VASP's density functional perturbation theory approach.

III. RESULTS AND DISCUSSION

A. Experimental observations

The ground-state structure of Li_2C_2, *Immm* Li_2C_2, relates to the antifluorite structure. Li atoms are coordinated by four dumbbell units and each dumbbell unit by eight Li ions. When recording Raman spectra of Li_2C_2 in a DAC, it was consistently observed that *Immm* Li_2C_2 transforms reversibly at around 15 GPa into a high-pressure modification. This is shown in Fig. 1.

The retention of the dumbbell units is evidenced by the persistence of the acetylide C-C stretching vibration (A_g). The stretching mode frequency drops discontinuously by about 20 cm^{-1} at the transition. At higher pressures the Raman spectra became featureless and remained featureless upon decompression. This phenomenon is attributed to irreversible amorphization of Li_2C_2 at high pressures [9]. In the Raman experiments no PTM was used in order to avoid any background scattering from possible surface contamination. The nonhydrostatic pressure conditions do not appear to influence the transition into the high-pressure modification. However, pressures at which irreversible amorphization occurs varied between 17 and 25 GPa.

Figure 2 shows synchrotron PXRD patterns of Li_2C_2 across the phase transition and up to 24.7 GPa. Different from the Raman studies, pressure conditions here were hydrostatic. Below 16 GPa patterns correspond to *Immm* Li_2C_2. At 16.5 GPa additional reflections appear. The onset pressure of

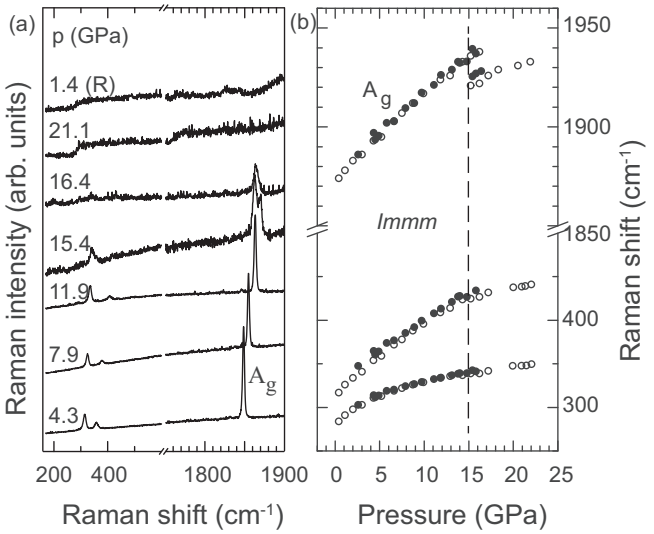

FIG. 1. (a) Raman spectra of polycrystalline Li_2C_2 at different pressures, (R) = decompression, and (b) observed mode frequencies as a function of pressure from two experiments (black and white circles, respectively). The broken vertical line marks the transition pressure for a reversible structural transformation. No PTM was used in order to avoid scattering by sample surface contaminations. Li_2C_2 amorphizes irreversibly at pressures between 17 GPa (black circle experiment) and 24 GPa (white circle experiment, according to Ref. [9]).

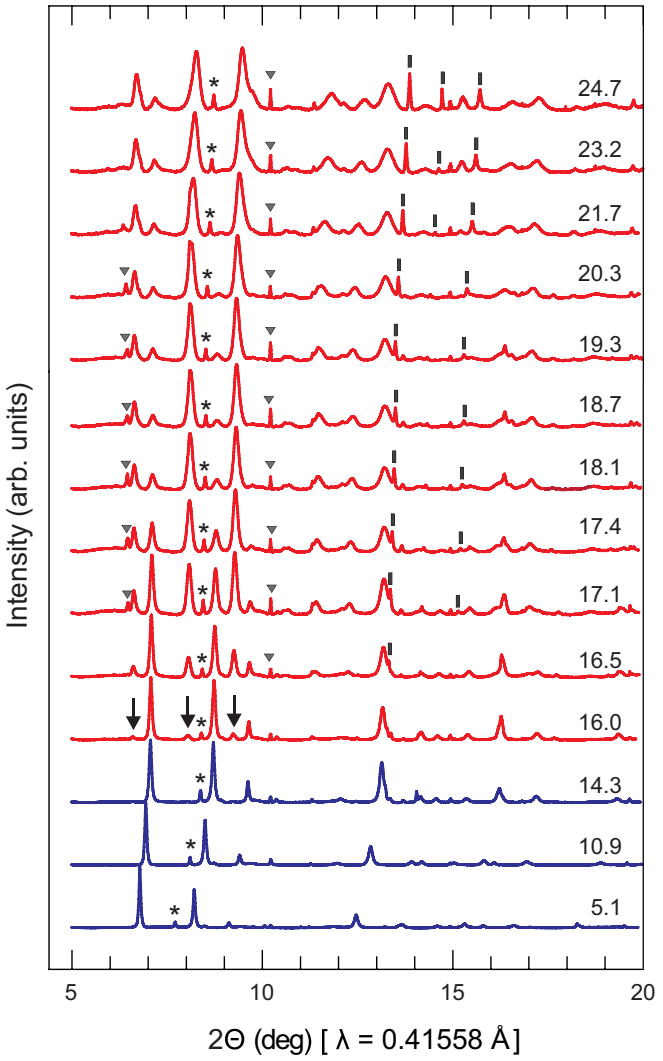

FIG. 2. (Color online) Compilation of x-ray diffraction patterns of Li_2C_2 ($\lambda = 0.41558$ Å) across the phase transition. Numbers are pressure in GPa. Blue patterns correspond to the pure *Immm* phase. The arrows mark the appearance of *Pnma* reflections. Asterisks mark a reflection from a graphite impurity. Triangles and bars mark reflections from ruby and the PTM He, respectively.

the phase transition is in good agreement with the Raman experiments. *Immm* Li_2C_2 coexists with the high-pressure modification as a nonequilibrium phase mixture beyond 20 GPa. The diffraction patterns taken at the highest applied pressure still indicated the presence of crystalline Li_2C_2, although reflections are broadened significantly. The data measured at 18.7 GPa were chosen for an *ab-initio* structure solution, as here the best resolution with respect to reflection overlaps with *Immm* Li_2C_2 and broadening of reflections was found. The new diffraction peaks could be indexed with a primitive orthorhombic unit cell ($a \approx 5.1$ Å, $b \approx 4.5$ Å, $c \approx 5.9$ Å), which pointed to $Z = 4$. Due to the overlap of reflections a space group could not be determined unambiguously, but whole pattern decomposition suggested assignment of *Pnma*. Using a direct-space approach [15] within this space group yielded a structural model that resembled the orthorhombic room temperature modification of Rb_2C_2 ($Z = 4$) [28].

B. Elucidation of *Pnma* Li_2C_2

To aid the structure elucidation, crystal structure searches by USPEX were performed at a target pressure of 20 GPa, well above the experimental transition pressure and below possible amorphization under hydrostatic conditions, respectively. Previous efforts using crystal-structure prediction methodology in the structure search for high-pressure Li_2C_2 have been restricted to simulation cells containing two formula units (i.e., eight atoms) [9]. This resulted in an energetically favorable structure (with $Cmc2_1$ symmetry) for pressures above 15 GPa. However, calculated frequencies of Raman active modes for $Cmc2_1$ Li_2C_2 deviated considerably from experiment. When extending the simulation cells to contain four formula units (16 atoms), as suggested by the diffraction experiments, the search indeed yielded a structure with *Pnma* symmetry. Figure 3 shows the enthalpy differences (with respect to the *Immm* ground-state structure) as a function of pressure for *Pnma* Li_2C_2 and earlier predicted $Cmc2_1$ Li_2C_2. At pressures around 13 GPa the enthalpy of *Pnma* Li_2C_2 becomes lower than the ground state. This value for the transition pressure is slightly lower than the experimental observation. The minor discrepancy may be attributed to the negligence of zero-point-energy contributions and temperature effects in our calculations. Importantly, *Pnma* Li_2C_2 is dynamically stable in the pressure range 10–30 GPa (see Supplemental Material [29], Fig. S1). The structural parameters at 20 GPa are compiled in Table I. Additionally, Ref. [29] contains parameters for the relaxed structures of *Immm* and *Pnma* Li_2C_2 for the complete investigated pressure range 0–40 GPa (Tables S1 and S2).

For Rietveld refinement the structural parameters of the model obtained with USPEX were used as starting parameters. The refined parameters for *Pnma* Li_2C_2 at 18.7 GPa are given in Table II. Details of the measurement and the refinement

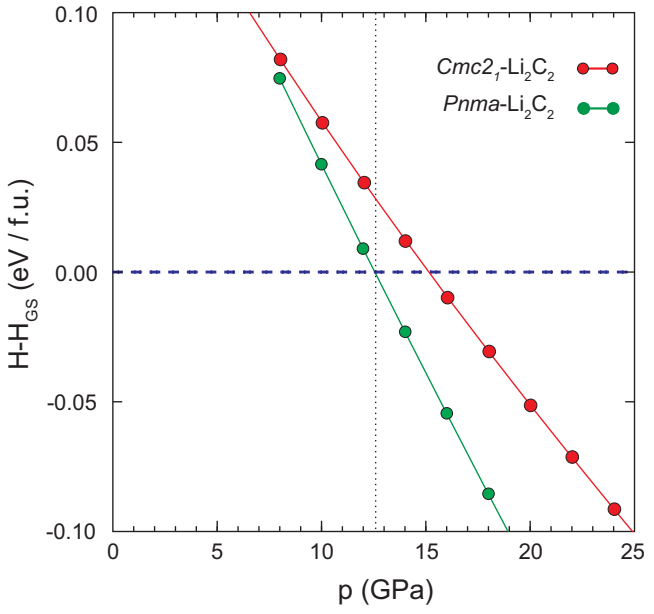

FIG. 3. (Color online) Calculated enthalpy-pressure relations (per formula unit) for Li_2C_2 with respect to the *Immm* ground-state structure. The dotted vertical line marks the transition pressure for the transformation to the *Pnma* high-pressure modification.

TABLE I. Structural parameters of *Pnma* Li_2C_2 at 20 GPa (DFT optimized).

Unit cell (Å)	$a = 5.0133$	$b = 4.4893$	$c = 5.8218$
Li_1 (4*c*)	$x = 0.1623$	$y = 0.25$	$z = 0.9033$
Li_2 (4*c*)	$x = 0.9945$	$y = 0.25$	$z = 0.2874$
C (8*d*)	$x = 0.7535$	$y = 0.1108$	$z = 0.9229$

are summarized in Table S3 [29]. In Table III interatomic distances are compared with those of the computed structure at 20 GPa. The refinement of the Li atom positions was quite unstable and led to a few short Li-Li distances. This can be attributed to the modest data quality and the strong overlap of reflections from coexisting *Immm* Li_2C_2. The reduced data quality could be a consequence of Li disorder, connected to the occurrence of an intermediate phase between *Immm* and *Pnma* Li_2C_2. Such an intermediate phase has been identified for the high-pressure-phase transition of Li_2S [30] which, as we will discuss later, relates closely to that of Li_2C_2. Also, an intermediate phase with varying Li disorder might explain the extended range of coexistence of *Immm* and *Pnma* Li_2C_2. However, such a phase could not be unambiguously identified from our diffraction data. The final fit of the 18.7 GPa data is shown in Fig. 4. Differences between the calculated and measured profiles (in particular, extra sharp reflections) can mainly be attributed to ruby and solid helium. Attempts to improve the fit by applying parameters for stress, strain, or anisotropic peak broadening gave unstable refinements and did not lead to physically meaningful results. Only the refinement of preferred orientation parameters (March-Dollase) gave a significant improvement of the fit. In Table S4 we also present the results from Rietveld refinements of the data at 7.2, 18.1, 18.7, and 19.3 GPa, respectively [29].

Figure 5 shows the pressure-volume (p-V) relations of *Immm* and *Pnma* Li_2C_2. Unit-cell parameters as a function of pressure from diffraction data are given in Tables S5 and S6 [29]. Both experimental and calculated p-V data were fitted to a three-parameter Birch-Murnaghan equation of state (EOS) expression [31]. Generally there is good agreement between calculated and experimentally determined p-V data. Computed volumes are somewhat underestimated, by 2%–2.5%. The first-order phase transition from *Immm* to *Pnma* Li_2C_2 is accompanied by a 7% volume reduction. The fitted EOS parameters are presented in Table IV. For *Immm* Li_2C_2 computed and experimental p-V data give virtually identical parameters. The ambient-pressure bulk modulus of this phase is around 40 GPa. For *Pnma* Li_2C_2 the bulk modulus extracted from the experimental data is 112 GPa at the reference pressure $p_r = 16.5$ GPa ($V_r = 34.5$ Å^3).

TABLE II. Structural parameters of *Pnma* Li_2C_2 at 18.7 GPa (Rietveld refinement).

Unit cell (Å)	$a = 5.098(2)$	$b = 4.505(1)$	$c = 5.909(2)$
Li_1 (4*c*)	$x = 0.144(4)$	$y = 0.25$	$z = 0.938(3)$
Li_2 (4*c*)	$x = 0.999(5)$	$y = 0.25$	$z = 0.227(5)$
C (8*d*)	$x = 0.742(1)$	$y = 0.1163(3)$	$z = 0.9100(6)$

TABLE III. Interatomic distances (Å) in *Pnma* Li_2C_2.

Atom pairs	Exp. structure (18.7 GPa)	Comp. structure (20 GPa)
Li_1–Li	1.86–2.68 Å (4×)	2.39–2.62 Å (4×)
Li_2–Li	1.86–2.68 Å (6×)	2.39–2.62 Å (6×)
Li_1–C	1.97 Å (2×), 2.14 Å (2×), 2.20 Å (2)	1.96 Å (2×), 2.05 Å (2), 2.15 Å (2×)
Li_2–C	2.26 Å (2×), 2.33 Å (2×), 2.36 Å (2×), 2.55 Å (2×)	2.19 Å (2×), 2.22 Å (2×), 2.39 Å (2×), 2.52 Å (2×)
C–C	1.20[a]	1.25
C–Li	1.97–2.55 (7×)	1.96–2.52 (7×)

[a]Soft constraints.

C. *Cmcm* Li_2C_2 and structural relationships

The high-pressure-phase *Pnma* Li_2C_2 amorphizes irreversibly in room temperature Raman experiments at ∼17 GPa (nonhydrostatic) but persists up to at least 25 GPa under hydrostatic conditions. Computationally, *Pnma* Li_2C_2 may be further compressed. Interestingly, as shown in Fig. 6, at around 32 GPa this yields a transition into another structure. The new structure is topologically equivalent to *Pnma* Li_2C_2 but adopts the higher-symmetry space group *Cmcm*. The structural parameters for *Cmcm* Li_2C_2 and their variation with pressure are compiled in Table S7 in Ref. [29]; EOS parameters are included in Table IV.

Figure 7 depicts the structural relations between ground-state *Immm* Li_2C_2 and the *Pnma* and *Cmcm* high-pressure

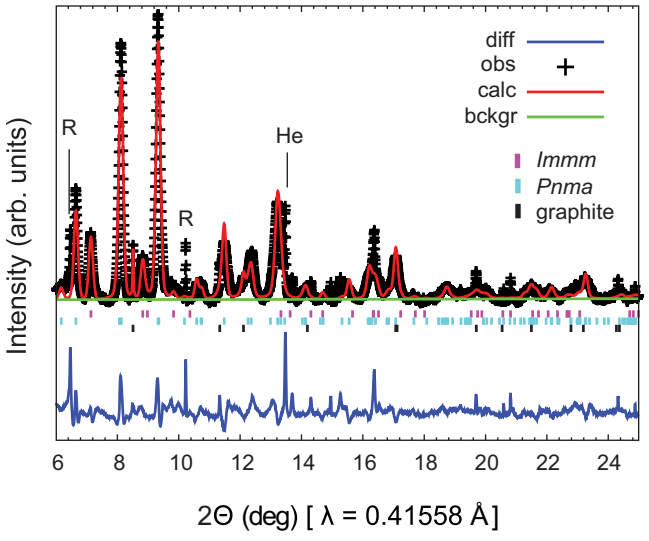

FIG. 4. (Color online) Rietveld refinement of the synchrotron PXRD pattern of *Pnma* Li_2C_2 at 18.7 GPa ($\lambda = 0.41558$ Å). Experimental data points (+), calculated profile (red solid line), and difference curve (blue curve below) are shown. Vertical bars mark the positions of Bragg reflections of graphite (black), *Pnma* Li_2C_2 (light blue), and *Immm* Li_2C_2 (magenta). Sharp extra reflections stem from ruby (R) and the PTM He.

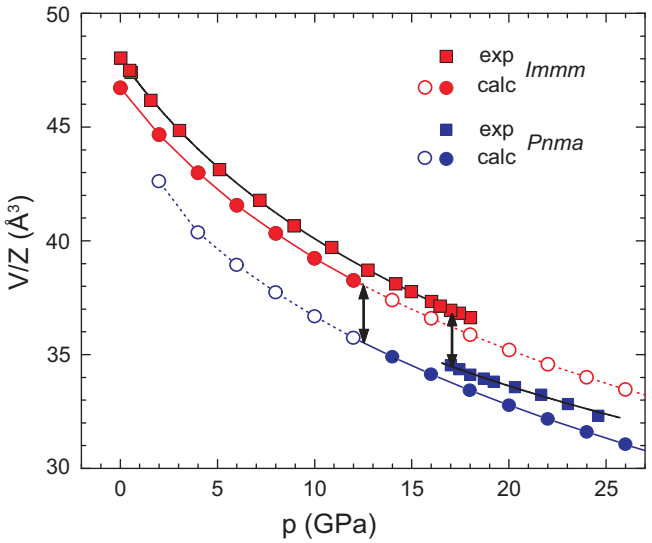

FIG. 5. (Color online) Volume versus pressure data for *Immm* Li_2C_2 (red symbols) and *Pnma* Li_2C_2 (blue symbols). Experimental and computed values are presented as squares and circles, respectively. The transition pressures are marked by arrows.

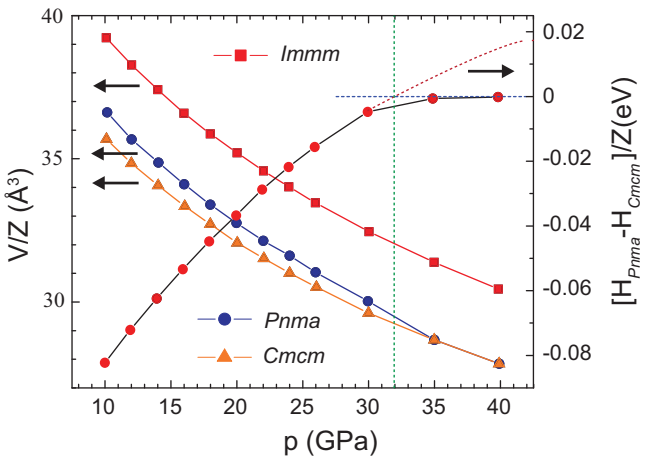

FIG. 6. (Color online) Volume-pressure relation (left ordinate) of the high-pressure phases *Pnma* Li_2C_2 and *Cmcm* Li_2C_2 (the *Immm* ground-state structure is included for comparison) and enthalpy-pressure relation of *Pnma* Li_2C_2 with respect to *Cmcm* Li_2C_2 (right ordinate). The dotted red line is a polynomial fit of H_{Pnma}-H_{Cmcm} to pressures < 30 GPa. The transition pressure is marked by a vertical line.

phases. As mentioned earlier, the *Immm* structure relates to the antifluorite type: C_2 dumbbells are arranged as a quasi-cubic close packing in which Li atoms occupy the tetrahedral voids. Consequently, each C_2 dumbbell is surrounded by eight Li atoms and each Li atom by four dumbbell units. Alternatively, the *Immm* structure can be viewed as a stacking of layers consisting of planar, rectangular nets formed by the Li ions which are stuffed by C_2 dumbbells oriented perpendicularly. Layers are stacked along the *b* direction (which is the elongation direction of dumbbells) and consecutive layers A and B are related by the *I* centering.

Also within *Pnma* Li_2C_2 Li ions form planar nets (parallel to the *ac* plane) that consist of triangle ribbons running along the *a* direction. Interatomic distances within triangles are short compared to distances in between (2.5 Å vs 3.1 Å at 20 GPa). Planar Li nets are completed to layers by perpendicularly oriented C_2 dumbbells interspersed between triangle ribbons. In the *Pnma* structure consecutive layers A and B are stacked in a way that C_2 dumbbells (e.g., in a layer A) attain a trigonal prismatic coordination by two triangles from adjacent layers above and below (layers B). A dumbbell is coordinated additionally by three Li ions which are situated in the same layer and cap the rectangular faces of the trigonal prism.

TABLE IV. Equation-of-state parameters for phases of Li_2C_2. Note that the experimental results for *Pnma* Li_2C_2 refer to a reference pressure of 16.5 GPa, not zero pressure.

Li_2C_2	V_0 (Å^3)	K_0 (GPa)	K_0'
Immm exp	47.9	39(1)	3.9(2)
Pnma exp	$V_r = 34.5$	$K_r = 112(5)$	4 (fixed)
Immm calc	46.7	40.8	3.9
Pnma calc	44.13	34.7	4.9
Cmcm calc	42.71	38.7	4.3

Consequently, compared to *Immm* Li_2C_2 the coordination of a dumbbell by Li ions is increased to 9.

As *Immm* Li_2C_2 relates to the antifluorite type so does the *Pnma* structure to the anticotunnite type. *Pnma* Li_2C_2 is isostructural to the recently discovered ternary carbides $CsKC_2$ and $CsRbC_2$ [32], and antifluorite–anticotunnite transitions are frequently observed for alkali metal chalcogenides A_2B at high pressures. In particular, Li_2O and Li_2S display this transition at around 45 and 12 GPa, respectively [30,33]. For Na_2S the antifluorite ground-state structure transforms to the anticotunnite structure at even lower pressures, at around 7 GPa. At about 16 GPa another transition takes place which results in a phase with the Ni_2In-type structure [34].

Interestingly, the sequence antifluorite → anticontunnite → Ni_2In type is also shown by Li_2C_2 as *Cmcm* Li_2C_2 relates to the hexagonal Ni_2In structure. The topology of planar Li-ion nets is identical in *Pnma* and *Cmcm* Li_2C_2. However, in the higher-symmetry *Cmcm* structure ribbons are straightened into distinct zigzag chains in which triangles are strictly oriented up and down [cf. Fig. 7(b)]. These chains run along the *c* direction. The orientation of triangles from adjacent chains yields five-membered rings which are centered by the dumbbell units. Because the trigonal prismatic environment of a dumbbell by Li triangles situated in layers above and below is maintained, its total coordination by Li ions is increased to 11 with respect to the *Pnma* structure. The coordination polyhedron corresponds to an Edshammar polyhedron, which is the signature of the Ni_2In structure type [35],

To conclude the discussion of structural relationships, we address the evolution of interatomic distances with pressure [referring to the density-functional theory (DFT) optimized structures]. The C-C distance within dumbbell units is only slightly compressible. Within the *Immm* structure this distance reduces from 1.256 Å at ambient pressure to 1.239 Å at 40 GPa. This is similar for the high-pressure forms. Here this

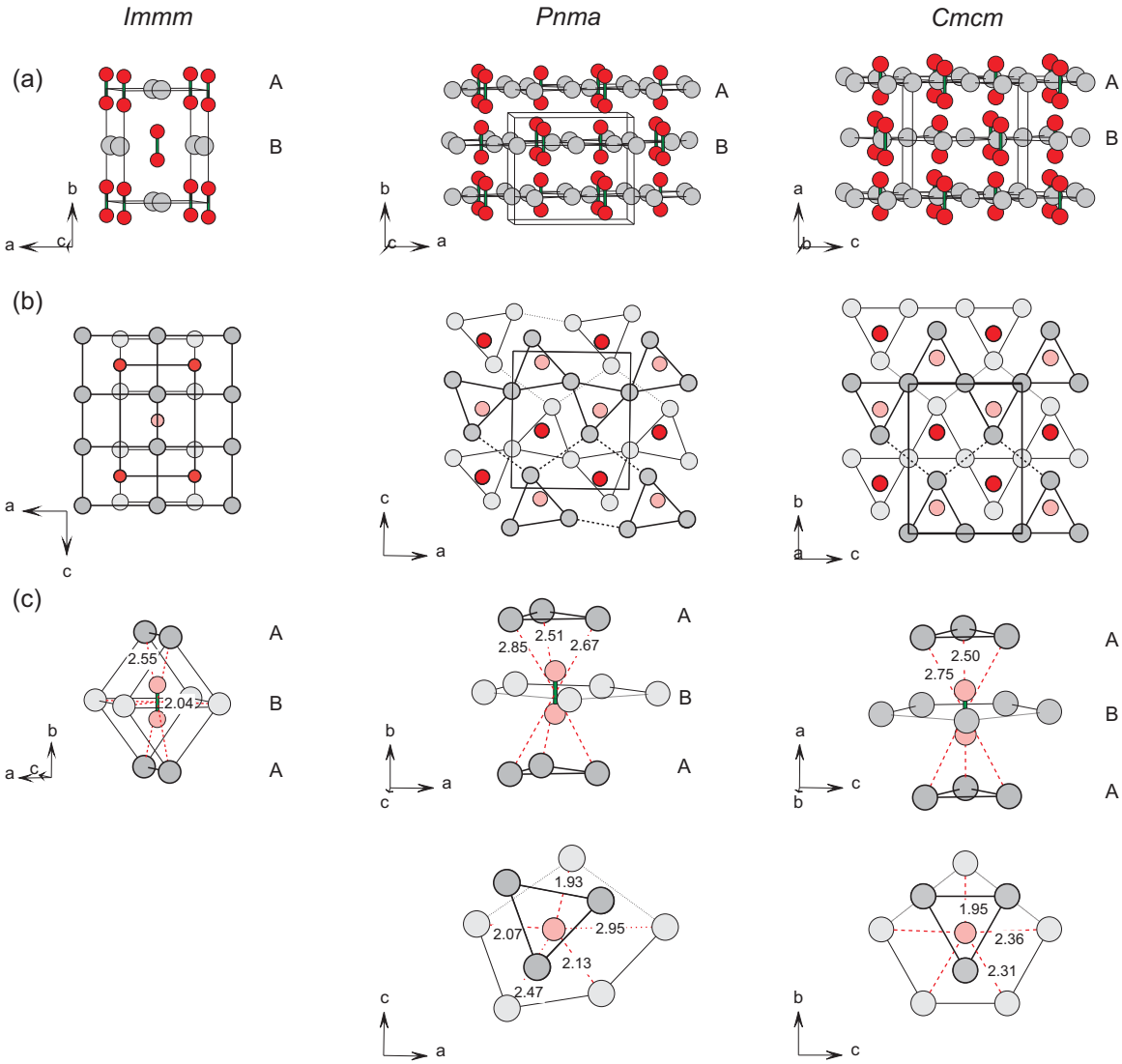

FIG. 7. (Color online) (a) Crystal structures of *Immm*, *Pnma*, and *Cmcm* Li_2C_2 represented as layers consisting of planar nets formed by Li ions, which are centered by perpendicularly oriented dumbbell units. Li ions are shown as light gray circles and C atoms as red circles. Layers are stacked with an AB sequence in the dumbbell direction, as described in the text. (b) View of the structures along the layer stacking direction. A-type layers are distinguished by bold lines. B-type layers by thin lines and pale colors. (c) Coordination of C_2 dumbbells within the three phases. The numbers indicate the distances between the dumbbell center and surrounding Li ions in Å (referring to DFT optimized structures at 20 GPa).

distance decreases from 1.254 Å at 10 GPa to 1.244 Å at 40 GPa. The Li-Li distances defining the coordination around C_2 dumbbells are 2.55, 2.81, and 3.02 Å for the *Immm* structure at ambient pressure. They reduce to 2.35, 2.58, and 2.84 Å at 14 GPa, which is close to the calculated transition pressure. At this pressure the corresponding Li-Li distances in the *Pnma* structure are between 2.46 and 3.17 Å.

D. Electronic structure changes with pressure

The band structures of *Immm* Li_2C_2 and *Pnma*/*Cmcm* Li_2C_2 are shown in Fig. 8. At pressures below 10 GPa both the ambient- and high-pressure forms exhibit insulating properties. At ambient pressure *Immm* Li_2C_2 has an indirect band gap of 3.3 eV, with the bottom of the conduction band at Γ and the top of the valence band at T. The valence bands mirror the molecular orbital (MO) diagram of the acetylide anion. Their topology for Li_2C_2 is similar to CaC_2, whose electronic structure has been studied earlier [36,37]. The weakly dispersed band centered at –12 eV below the Fermi level corresponds to the $sp\sigma_g$ bonding MO. Bands corresponding to the two lone-pair states ($sp\sigma_u$ and $sp\sigma_g$) have dispersions of about 2 eV and are located in the range –4 to –1 eV below the Fermi level. The two π-bonding bands constitute the top of the valence band. It is clearly seen that pressure increases especially in the lone-pair–Li interactions because the dispersion of lone-pair–based bands increases most. The pressure dependence of the DFT-GGA–computed band gap is shown in Fig. 9. It decreases linearly, but *Immm* Li_2C_2 obviously stays insulating.

At low pressure (below 10 GPa) *Pnma* Li_2C_2 exhibits an indirect band gap of <2.5 eV with the bottom of the

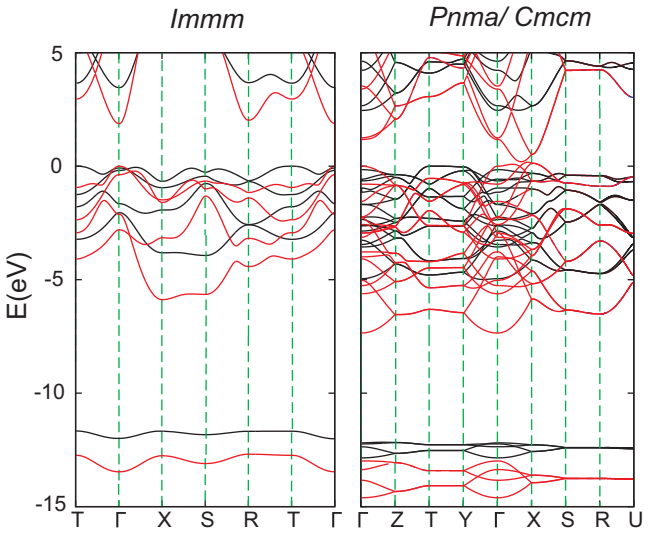

FIG. 8. (Color online) Calculated band structures of the ground-state (left) and the higher-pressure phases (right) of Li_2C_2. Black lines represent the ground-state and *Pnma* high-pressure phase at 0 and 8 GPa, respectively. Red lines represent the ground-state and *Cmcm* high-pressure phase at 40 GPa.

conduction band at Γ and the top of the valence band lying along T-Y. The band gap of *Pnma* Li_2C_2 diminishes faster with pressure compared to the *Immm* structure. In high-pressure Raman experiments a darkening of the sample is observed after the *Immm*-to-*Pnma* phase transition [9]. This possibly relates to the considerably decreased band gap of *Pnma* Li_2C_2. At 35 GPa the *Pnma* structure merged into the *Cmcm* structure. At this pressure the calculated band gap dropped below 0.5 eV. Above 40 GPa the band gap of *Cmcm* Li_2C_2 has closed. The comparatively low pressure for (hypothetical) metallization of an ionic structure is remarkable. The changed pressure dependence of the band gap for the high-pressure phases (compared to *Immm* Li_2C_2) can be attributed to the different coordination of dumbbell units. In the high-pressure phases

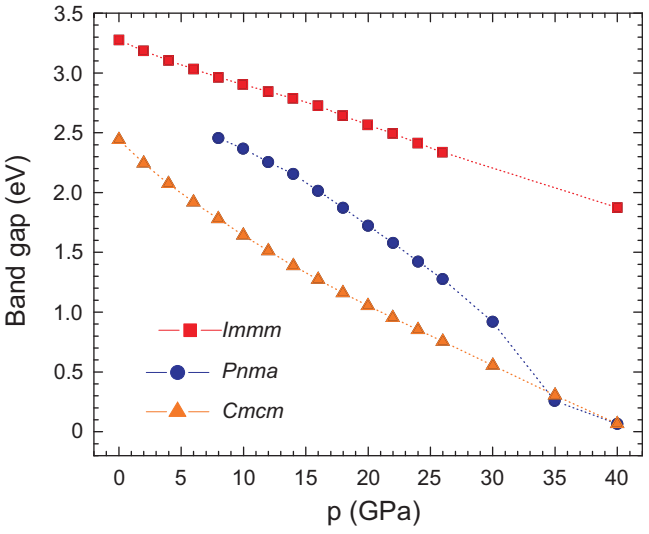

FIG. 9. (Color online) Band gap–pressure relations of the ground-state and high-pressure phases of Li_2C_2.

acetylide lone pairs are coordinated by triangles of Li ions. With pressure this coordination will develop into a covalent bonding interaction between C and Li, formally corresponding to electron donation from the dumbbell C_2^{2-} to Li^+, and eventually leading to metallization.

IV. CONCLUSIONS

In summary, we have employed a combination of synchrotron x-ray diffraction experiments and computational evolutionary search methodology to elucidate the high-pressure crystal structure of the acetylide carbide Li_2C_2. The observed high-pressure phase has *Pnma* symmetry and relates to the anticotunnite structure ($Z = 4$). In hydrostatic experiments *Pnma* Li_2C_2 does not amorphize under pressures up to 25 GPa. We find that if *Pnma* Li_2C_2 were prevented from amorphization it would transform at around 32 GPa to a higher-symmetry *Cmcm* structure that is closely related to the Ni_2In type. *Cmcm*-Li_2C_2 would metallize at pressures above 40 GPa as a result of indirect band overlap. The sequence antifluorite → anticotunnite → Ni_2In–type mirrors a common trend of high-pressure-phase transitions in A_2B compounds toward higher coordination.

We point out that the high-pressure behavior of the acetylide carbides Li_2C_2 and MC_2 (M = Ca, Sr, Ba) appears strikingly similar to the corresponding sulfides. Experimental and/or calculated transition pressures for the sequences antifluorite → anticotunnite → Ni_2In–type (referring to Li_2C_2/Li_2S) and rock salt → CsCl–type (referring to MC_2/MS) are remarkably close [38–43]. This may be attributed to a similar polarizability of the C_2^{2-} and S^{2-} anions. However, unlike sulfides, acetylides will undergo amorphization with pressure and expected phase transitions may not be observed. The origin of the pressure-induced amorphization of acetylides is uncertain, and different scenarios can be envisioned. For example, amorphization could indicate compositional instability and phase segregation, which appears to be the case for BaC_2 [5]. Furthermore, it could connect with a pressure limit for stability of multiple bonded light element entities, as suggested in Ref. [7]. However, the enthalpic pressure limit for the stability of C_2^{2-} units is rather low, as computations show clearly that with pressure carbides with polymeric anions become rapidly favored over acetylides. Specifically, for Li_2C_2 a phase with the CrB structure becomes more stable than *Immm* Li_2C_2 at already 5 GPa [2,3] This is far below the experimentally observed *Immm*-to-*Pnma* phase transition (see also Fig. S2 in Ref. [29]) and it has been concluded that acetylides are distinguished by a high kinetic stability [3]. The elucidation of the origin of the kinetic stability and pressure-induced amorphization of acetylides will require the analysis of the composition and local structure of the amorphous carbides by, e.g., synchrotron extended x-ray absorption fine structure (EXAFS) and/or total scattering experiments, preferably in combination with molecular dynamics simulations.

ACKNOWLEDGMENTS

This work was supported by the Swedish Research Council through Grant No. 2012-2956 and the National Science Foundation through Grant No. DMR-1007557.

[1] U. Ruschewitz, Coord. Chem. Rev. **244**, 115 (2003).

[2] X.-Q. Chen, C. Fu, and C. Franchini, J. Phys.: Condens. Matter **22**, 292201 (2010).

[3] D. Benson, Y.-L. Li, W. Luo, R. Ahuja, G. Svensson, and U. Häussermann, Inorg. Chem. **52**, 6402 (2013).

[4] Y.-L. Li, W. Luo, Z. Zeng, H.-Q. Lin, H.-k. Mao, and R. Ahuja, Proc. Natl. Acad. Sci. USA **110**, 9289 (2013).

[5] D.-H. Wang, H.-Y. Zhou, C.-H. Hu, A. R. Oganov, Y. Zhong, and G.-H. Rao, Phys. Chem. Chem. Phys. **16**, 20780 (2014).

[6] Y.-L. Li, R. Ahuja, and H.-Q. Lin, Chin. Sci. Bull. **59**, 5269 (2014); Y.-L. Li, S.-N. Wang, A. R. Oganov, H. Gou, J. S. Smith, and T. A. Strobel, Nat. Commun. **6**, 6974 (2015).

[7] I. Efthimiopoulos, K. Kunc, G. V. Vazhenin, E. Stavrou, K. Syassen, M. Hanfland, St. Liebig, and U. Ruschewitz, Phys. Rev. B **85**, 054105 (2012).

[8] I. Efthimiopoulos, G. V. Vazhenin, K. Kunc, E. Stavrou, K. Syassen, M. Hanfland, S. Liebig, and U. Ruschewitz, in *Book of Abstracts*, 50th EHPRG Meeting, Thessaloniki (2012), p. 224; I. Efthimiopoulos, G. Vajenine, E. Stavrou, K. Kunc, K. Syassen, S. Liebig, U. Ruschewitz, and M. Hanfland *European Crystallography Meeting, ECM26*, Darmstadt (2010).

[9] J. Nylén, S. Konar, P. Lazor, D. Benson, and U. Häussermann, J. Chem. Phys. **137**, 224507 (2012).

[10] Q. Zhu, A. R. Oganov, C. W. Glass, and H. T. Stokes, Acta Crystallogr. Sect. B **68**, 215 (2012).

[11] K. Syassen, High Press. Res. **28**, 75 (2008).

[12] A. P. Hammersley, S. O. Svensson, M. Hanfland, A. N. Fitch, and D. Hausermann, High Press. Res. **14**, 235 (1996).

[13] WINXPOW, Stoe & Cie GmbH, Darmstadt (2010).

[14] A. Boultif and D. Louër, J. Appl. Crystallogr. **24**, 987 (1991).

[15] H. Putz, J. Schön, and M. Jansen, J. Appl. Crystallogr. **32**, 864 (1999).

[16] A. C. Larson and R. B. Von Dreele, General Structure Analysis System (GSAS), Los Alamos National Laboratory Technical Report LAUR 86-748 (2004).

[17] A. R. Oganov and C. W. Glass, J. Chem. Phys. **124**, 244704 (2006).

[18] C. W. Glass, A. R. Oganov, and N. Hansen, Comput. Phys. Commun. **175**, 713 (2006).

[19] A. O. Lyakhov, A. R. Oganov, H. T. Stokes, and Q. Zhu, Comput. Phys. Commun. **184**, 1172 (2013).

[20] R. C. Hoft, J. D. Gale, and M. J. Ford, Mol. Simul. **32**, 595 (2006).

[21] J. M. Soler, E. Artacho, J. D. Gale, A. García, J. Junquera, P. Ordejón, and D. Sánchez-Portal, J. Phys.: Condens. Matter **14**, 2745 (2002).

[22] J. P. Perdew, K. Burke, and M. Ernzerhof, Phys. Rev. Lett. **77**, 3865 (1996).

[23] N. Troullier and J. L. Martins, Phys. Rev. B **43**, 1993 (1991).

[24] G. Kresse and J. Furthmüller, Phys. Rev. B **54**, 11169 (1996).

[25] P. E. Blöchl, Phys. Rev. B **50**, 17953 (1994); G. Kresse and D. Joubert, *ibid.* **59**, 1758 (1999).

[26] H. J. Monkhorst and J. D. Pack, Phys. Rev. B **13**, 5188 (1976).

[27] P. E. Blöchl, O. Jepsen, and O. K. Andersen, Phys. Rev. B **49**, 16223 (1994).

[28] U. Ruschewitz, P. Müller, and W. Kockelmann, Z. Anorg. Allg. Chem. **627**, 513 (2001).

[29] See Supplemental Material at http://link.aps.org/supplemental/10.1103/PhysRevB.92.064111 for (1) DFT optimized structure parameters for *Immm*, *Pnma*, and *Cmcm* Li_2C_2 for the pressure range 0–40 GPa; (2) details of the structural investigation and selected crystallographic parameters of Li_2C_2 at 18.7 GPa; (3) comparison of DFT optimized and experimental structure parameters (Rietveld fits) at 7.2, 18.1, 18.7, and 19.3 GPa; (4) experimental lattice parameters for *Immm* and *Pnma* Li_2C_2 (Le Bail fits); (5) dispersion relation and corresponding phonon density of states of *Pnma* Li_2C_2 at 20 GPa; (6) enthalpy-pressure relations of *Pnma* Li_2C_2 and Li_2C_2 with a CrB-type polycarbide structure.

[30] A. Grzechnik, A. Vegas, K. Syassen, I. Loa, M. Hanfland, and M. Jansen, J. Solid State Chem. **154**, 603 (2000).

[31] F. Birch, Phys. Rev. **71**, 809 (1947).

[32] S. Liebig, M. Paulus, C. Sternemann, and U. Ruschewitz, Z. Anorg. Allg. Chem. **639**, 2804 (2013).

[33] K. Kunc, I. Loa, A. Grzechnik, and K. Syassen, Phys. Status Solidi B **242**, 1857 (2005).

[34] A. Vegas, A. Grzechnik, K. Syassen, I. Loa, M. Hanfland, and M. Jansen, Acta Crystallogr. Sect. B **57**, 151 (2001); A. Vegas and M. Jansen, *ibid.* **58**, 38 (2002). D. Santamaria-Perez, A. Vegas, C. Muehle, and M. Jansen, *ibid.* **67**, 109 (2011).

[35] B. G. Hyde and S. Andersson, *Inorganic Crystal Structures* (Wiley, New York, 1989).

[36] E. Ruiz and P. Alemany, J. Phys. Chem. **99**, 3114 (1995).

[37] J. R. Long, R. Hoffmann, and H. J. Meyer, Inorg. Chem. **31**, 1734 (1992).

[38] J. Schön, Ž. Čančarević, and M. Jansen, J. Chem. Phys. **121**, 2289 (2004).

[39] S. Yamaoka, O. Shimomura, H. Nakazawa, and O. Fukunaga, Solid State Commun. **33**, 87 (1980).

[40] Y.-L. Lu and H. Zhao, Mod. Phys. Lett. B **28**, 1450190 (2014).

[41] A. Kulkarni, K. Doll, J. Schön, and M. Jansen, J. Phys. Chem B **114**, 15573 (2010).

[42] K. Syassen, Phys. Status Solidi A **91**, 11 (1985).

[43] H. Luo, R. G. Greene, K. Ghandehari, T. Li, and A. L. Ruoff, Phys. Rev. B **50**, 16232 (1994).